Discrimination between strain and temperature by cascading single-mode thin-core diameter fibers

Jie Shi, Shilin Xiao,* Miehua Bi, Lilin Yi, and Pei Yang

State Key Lab of Advanced Optical Communication Systems and Networks, Department of Electronics and Engineering, Shanghai Jiao Tong University, 800 Dongchuan Rd., Shanghai 200240, China

*Corresponding author: slxiao@sjtu.edu.cn

Received 29 November 2011; revised 4 February 2012; accepted 6 February 2012; posted 6 February 2012 (Doc. ID 159047); published 10 May 2012

A simple fiber-optic sensor capable of discrimination between temperature and strain is proposed and experimentally demonstrated. The sensor head is formed by cascading two sections of single-mode thin-core diameter fibers (TCFs) that act as two different inter-modal interferometers (IMIs). Due to the different sensitivity responses of the two IMIs to strain and temperature, it is possible to discriminate temperature and strain by monitoring the resonant wavelength shifts. The experimental results indicate that the measured strain and temperature resolutions are 37.41 $\mu\varepsilon$ and 0.732 °C within a strain range of 0–1333.3 $\mu\varepsilon$ and a temperature range from 26.9 °C to 61.7 °C. The sensing sensitivities of strain and temperature are −1.03 pm/$\mu\varepsilon$ and 30.74 pm/°C, respectively. The proposed sensor features the advantages of easy fabrication, low cost and high sensitivity, and it exhibits great potential in dual-parameter measurement.

OCIS codes: 060.2370, 060.2310.

1. Introduction

Fiber-optic sensors for discriminating two concurrent perturbations such as strain and temperature have been extensively investigated. These fiber-optic sensors are usually based on detecting two physical parameters that have different sensitivities to strain and temperature. Many designs by using fiber Bragg gratings (FBGs) and long period gratings (LPGs), such as one tilted FBG [1,2], a FBG written on the splice joint between two fibers [3,4], a superstructure FBG [5], and a FBG combined with a LPG [6], have been proposed. In addition, two superimposed fiber gratings with different Bragg wavelengths have been studied for simultaneous measurement of strain and temperature [7]. The first and second-order diffraction of a single Bragg grating has been demonstrated to decouple the effects of temperature and strain [8]. An optical rosette incorporating Bragg gratings has also been proposed to discriminate between strain and temperature [9]. Alternatively, the high-birefringence fiber loop mirror has attracted much attention for its applications in simultaneous measurement of strain and temperature. Different configurations of high-birefringence fiber loop mirror were reported to discriminate temperature and strain, such as using two sections of different types of high-birefringence fiber in a sagnac loop [10], two different concatenated high-birefringence fiber loop mirrors [11] and a high-birefringence fiber loop mirror with a FBG or a LPG [12,13]. However, grating-based sensors (FBG, LPG) always require precise and expensive phase masks and photolithographic procedures. A high-birefringence fiber loop mirror is composed of a 3 dB coupler, a polarization controller, a section of high-birefringence fiber and some single-mode fibers. Hence the high-birefringence fiber loop mirror generally has large footprint, which means it is hard to make a compact sensor.

Recently, in-line inter-modal interferometers (IMIs) have been intensively studied in optical

1559-128X/12/142733-06$15.00/0

sensing field because of its advantages of low-cost, small size and high sensitivity. Several technologies have been used to form the in-line IMIs, such as by using core mismatch [14,15], fiber tapers [16], and photonic crystal fiber [17]. The in-line IMIs have also been studied for discrimination of strain and temperature. Zhou *et al.* investigated a configuration by connecting a multimode fiber based IMI and a FBG for temperature and strain measurement [18]. Dong *et al.* proposed an all-fiber sensor by using a photonic crystal fiber IMI and a FBG [19].

In this paper, we propose and experimentally demonstrate a cost-effective fiber sensor for simultaneous measurement of strain and temperature by using in-series single-mode thin-core fibers (TCF) based IMIs. The single-mode TCFs used are commercial fibers and the whole fabrication process is only fiber splicing, therefore, the proposed sensing structure is low-cost and easy to implement. The sensing sensitivities of strain and temperature are -1.03 pm/$\mu\varepsilon$ and 30.74 pm/°C, respectively. The proposed sensor also features the advantages of high sensitivity, small size, and high stability.

2. Operation Principle

Figure 1 shows the schematic configuration of the in-series TCFs-based sensor. Two sections of uncoated single-mode TCFs (TCF-A & TCF-B) are spliced in series by a fiber fusion splicer, and acting as two different inter-modal interferometers (IMIs). At the SMF-TCF interface 1, part of light is coupled to the cladding of the TCF as cladding modes due to mode mismatch. After propagating through the TCF, the excited cladding modes will be re-coupled to the core of the SMF at the spliced point 2. The cladding modes interfere with the core mode due to the phase difference, thus the IMI-A is constructed. Similarly, IMI-B is constructed by TCF-B. Slightly core offsets between the TCF and SMF are made to get a high extinction ratio transmission spectrum.

After propagating through the TCF with the length of L, the phase difference Φ^j between the core and the cladding modes can be written as

$$\Phi^j = \frac{2\pi(n_{\text{core}}^{\text{eff}} - n_{\text{cl},j}^{\text{eff}})L}{\lambda} = \frac{2\pi\Delta n_j^{\text{eff}} L}{\lambda}, \tag{1}$$

where $n_{\text{core}}^{\text{eff}}$ and $n_{\text{cl},j}^{\text{eff}}$ are the effective refractive indices of the core and the jth cladding modes, respectively; Δn_j^{eff} is the effective refractive index difference between the core mode and the jth cladding mode, and λ is the light wavelength in vacuum. The free spectral range (FSR) of the interfering spectrum can be approximately written as:

$$\text{FSR} \approx \frac{\lambda}{\Delta n_j^{\text{eff}} L}. \tag{2}$$

As shown from Eq. (2), the FSR of the TCF-based IMI dependent on interference length L and the effective refractive index difference between the core and cladding modes.

The TCFs used are commercial fibers (Yangtze Ltd., BI & CS980). The TCF-A and B have the core/cladding diameters of 4.8/125 μm and 5.1/125 μm, and the cut-off wavelengths are 1260 nm and 964 nm, respectively. An Ericsson fusion splicer (Modal FSU 975), with a built-in core-offset attenuator program, was used to produce the core offset between the SMF and the TCF. The core offset is ~5 μm. Several IMIs were fabricated with different lengths of TCFs, and the typical transmission spectra are shown in Fig. 2. The length of TCF-A and TCF-B are approximately 16 mm and 20 mm, respectively. The maximum extinction ratio of the transmission spectrum is ~15 dB. As can be seen from Fig. 2, the spectra are a little inhomogeneous. It is because that more than one cladding modes are available in the interference pattern. We assume that only one cladding mode is dominantly excited, and other cladding modes are also excited but weakly. So, the main interference pattern is mainly formed by the core mode and the dominant cladding mode. Other weak cladding modes will slightly change the main interference pattern.

The interference patterns of the IMIs shown in Fig. 2 were Fourier transformed to obtain the spatial frequency, as shown in Fig. 3. Figure 3 shows that, beside the core modes, both IMIs have only one dominant peak in spatial frequency spectra, which means there is indeed one dominantly cladding mode, along with other weak cladding modes. Take the IMI formed by TCF-A as an example, the dominant

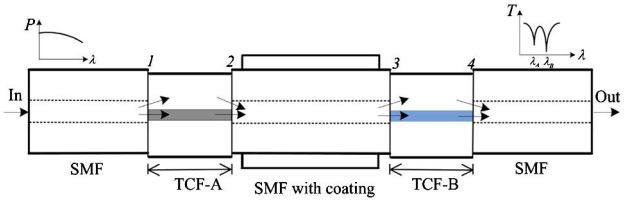

Fig. 1. (Color online) Schematic diagram of the in-series TCF-based sensor.

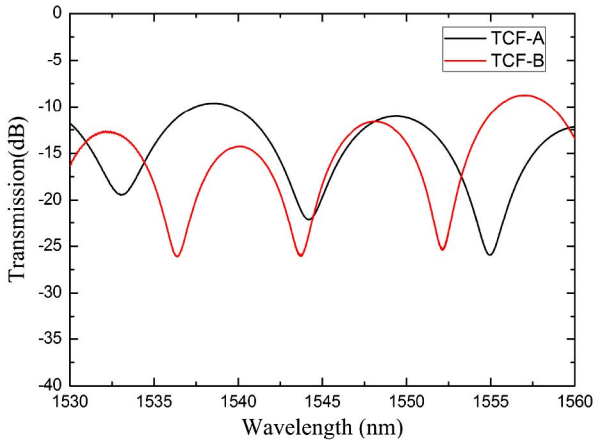

Fig. 2. (Color online) Measured transmission spectra of the IMIs fabricated by TCF-A and TCF-B.

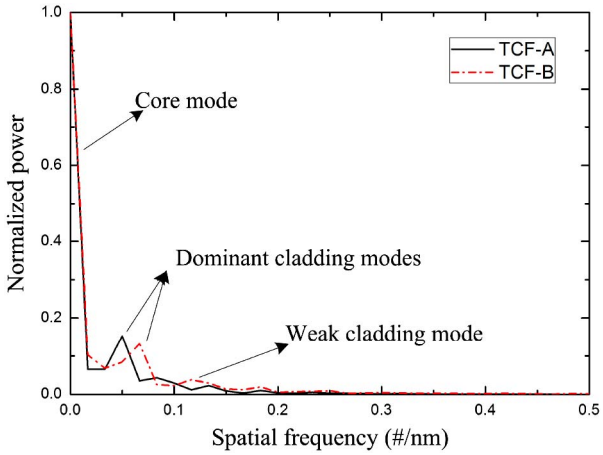

Fig. 3. (Color online) Spatial frequency spectra of the IMIs formed by TCF-A and TCF-B.

cladding mode locates at the spatial frequency of 0.05 #/nm, but the other cladding modes at spatial frequencies of 0.083 #/nm and 0.133 #/nm are weakly excited. So the interference pattern is mainly formed by the core mode and the dominant cladding mode, and the interference pattern is slightly modified by the weak cladding modes. Several IMIs with different lengths of TCFs were fabricated, and the free spectral ranges (FSRs) were measured and shown in Fig. 4(a) and (b). It can be seen that the FSR is inversely proportional to the interference length, which is consistent with Eq. (2). Fig. 4 also shows that the FSR responses to the length between TCF-A and TCF-B are different. It is because that the effective refractive index difference between the core mode and cladding modes of the TCF-A is different from that of TCF-B. The two TCFs used are commercial fibers, and they have different geometry and material composition in the fiber core, thus resulting in different effective refractive index difference.

When strain is applied to the IMI or the ambient temperature changes, the fiber length of the TCF and the effective RI difference between the core and dominant cladding modes change, therefore, the resonant wavelength will has a shift of $\Delta\lambda$. Because the core and cladding modes propagate in different waveguide structures in the TCF, the temperature and strain must affect the two modes in different manners. The wavelength response $\Delta\lambda$ of the IMI to temperature and strain can be given as $\Delta\lambda = K_\varepsilon\Delta_\varepsilon + K_T\Delta T$, where $K\varepsilon = [1 + (p_{e1} - p_{e2}n_2)/(n_1 - n_2)]$; $K_T = [\alpha + (\xi_1 n_1 - \xi_2 n_2)/(n_1 - n_2)]$ [20]; n_1 and n_2 are effective refractive indices of the core and cladding modes; p_{e1}, p_{e2} and ξ_1, ξ_2 are the photo-elastic constants and thermo-optic coefficients of the two modes, and α is the thermal expansion coefficients of the TCF. For the strain and temperature change of $\Delta\varepsilon$ and ΔT, the resonant wavelength shifts of the IMI-A and IMI-B can be expressed as

$$\begin{bmatrix} \Delta\lambda_A \\ \Delta\lambda_B \end{bmatrix} = \begin{bmatrix} K_{A\varepsilon} & K_{AT} \\ K_{B\varepsilon} & K_{BT} \end{bmatrix}, \tag{3}$$

where $\Delta\lambda_A$ and $\Delta\lambda_B$ are wavelength shift of IMI-A and IMI-B; $K_{A\varepsilon}$, K_{AT} and $K_{B\varepsilon}$, K_{BT} are the strain and temperature sensitivities of IMI-A and IMI-B, respectively. The applied strain and the temperature change can be simultaneously obtained from Eq. (4):

$$\begin{bmatrix} \Delta\varepsilon \\ \Delta T \end{bmatrix} = \frac{1}{M}\begin{bmatrix} K_{BT} & -K_{AT} \\ -K_{B\varepsilon} & K_{A\varepsilon} \end{bmatrix}\begin{bmatrix} \Delta\lambda_A \\ \Delta\lambda_B \end{bmatrix}, \tag{4}$$

where $M = K_{A\varepsilon}K_{BT} - K_{AT}K_{B\varepsilon}$. For given wavelength measurement resolutions of $\delta(\Delta\lambda_A)$ and $\delta(\Delta\lambda_B)$, the strain and temperature resolutions can be described as Eq. (5) [21]:

$$\begin{bmatrix} \delta(\Delta\varepsilon) \\ \delta(\Delta T) \end{bmatrix} = \frac{1}{|M|}\begin{bmatrix} |K_{BT}| & |K_{AT}| \\ |K_{B\varepsilon}| & |K_{A\varepsilon}| \end{bmatrix}\begin{bmatrix} \delta(\Delta\lambda_A) \\ \delta(\Delta\lambda_B) \end{bmatrix}. \tag{5}$$

The sensing sensitivities $K_{A\varepsilon}$, K_{AT} and $K_{B\varepsilon}$, K_{BT} can be obtained by the experiment.

3. Experiment and Discussion

Fig. 5 shows the schematic configuration of the experimental setup. A broadband source (BBS) was used as the light source. The transmission spectrum was measured by the optical spectrum analyzer (OSA) with the wavelength resolution of 10 pm. The IMI-A and IMI-B were fabricated by 17 mm long TCF-A and 22 mm long TCF-B, respectively. One side of IMI-A was fixed on a fiber holder, and the other side was fixed on a translation stage with a resolution of 10 μm. Both the IMI-A and IMI-B were

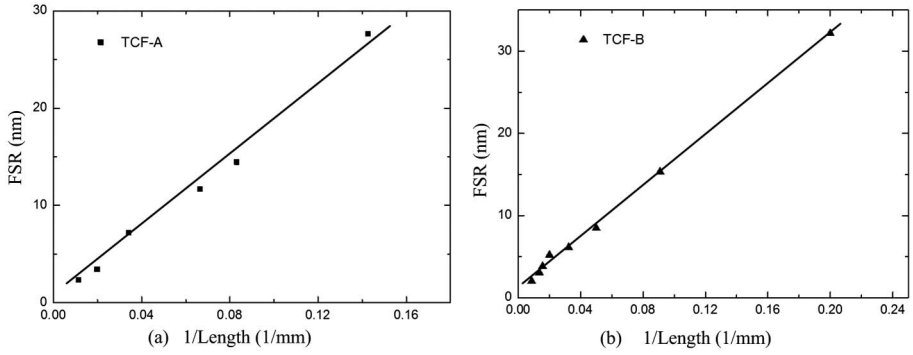

Fig. 4. Measured FSR of the IMI with respect to the length of TCF: (a) IMIs fabricated by TCF-A; (b) IMIs fabricated by TCF-B.

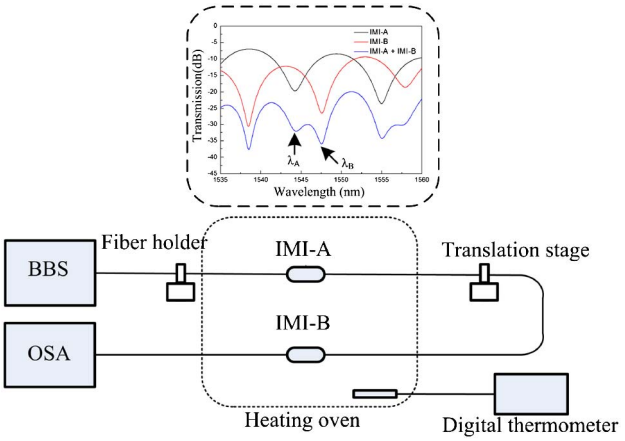

Fig. 5. (Color online) Schematic configuration of the experimental setup; the inset shows the transmission spectra of the IMI-A (black), IMI-B (red), and IMI-A concatenating IMI-B (blue).

placed in a heating oven, and a digital thermometer was used to monitor the temperature variation. The IMI-A was applied by both strain and temperature, while the IMI-B was only affected by temperature. The inset of Fig. 5 shows the transmission spectra of the IMI-A, IMI-B and IMI-A concatenating with IMI-B. When the two IMIs are connected in series, the transmission spectra of IMI-A and IMI-B are superimposed, while the resonant wavelengths λ_A of the IMI-A and λ_B of the IMI-B can also be clearly measured by the OSA. When the ambient temperature and strain change, the resonant wavelengths have corresponding shifts. By measuring the wavelength shifts of λ_A and λ_B, the variations of strain and temperature can be simultaneously determined.

In order to obtain the strain and temperature coefficients, strain and temperature changes were applied to the two IMIs separately. We first measured the strain response with respect to strain change in the range of 0–1333.3 $\mu\varepsilon$. Fig. 6(a) shows the measured spectral response to strain of IMI-A. With the increase of strain, the resonant wavelength λ_A shifted to the shorter wavelength, while the resonant wavelength λ_B stayed in the same value. The wavelength shift of λ_A has a linear relationship with the variation of strain; the correlation coefficient squares reached 0.996, as shown in Fig. 6(b). The strain sensitivities of IMI-A was −1.03 pm/$\mu\varepsilon$.

The ambient temperature was changed from 26.9 °C to 61.7 °C under zero strain. With the increase of the ambient temperature, both the transmission spectra of IMI-A and IMI-B experienced red shift, as shown in Fig. 7(a). Fig. 7(b) shows the measured wavelength shifts of IMI-A and IMI-B as functions of temperature. It can be seen that the resonant wavelength shifts of IMI-A and IMI-B have a good liner behavior with the variation of temperature, and the correlation coefficient squares of 0.996 and 0.994 were obtained. Therefore, the temperature sensitivities of IMI-A and IMI-B were 30.74 pm/°C and 20.48 pm/°C. The two TCFs show

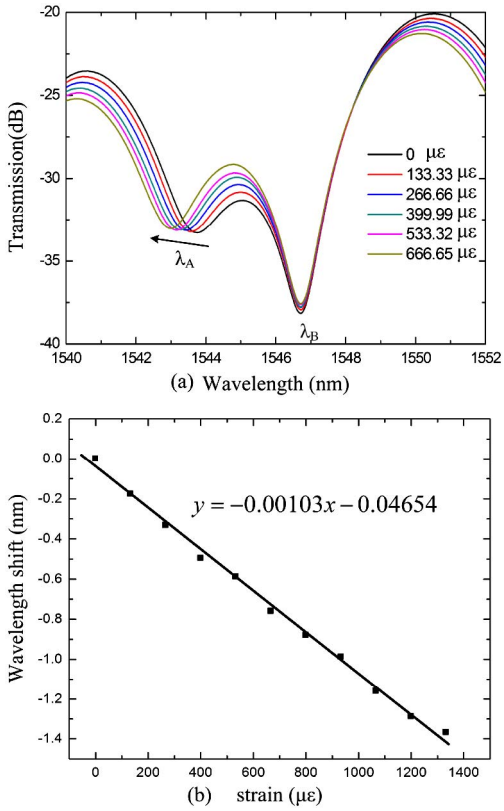

Fig. 6. (Color online) (a) Measured spectral response to strain; (b) The resonant wavelength shift of the IMI-A as a function of strain.

different temperature sensitivities due to their different material composition in fibers.

With the above experimental results, the variations of strain and temperature can be measured by

$$\begin{bmatrix} \Delta\varepsilon \\ \Delta T \end{bmatrix} = \frac{1}{-21.09}\begin{bmatrix} 20.48 & -30.74 \\ 0 & -1.03 \end{bmatrix}\begin{bmatrix} \Delta\lambda_A \\ \Delta\lambda_B \end{bmatrix}. \quad (6)$$

For the wavelength resolution of 10 pm, the resolutions of strain and temperature can be calculated by Eq. (5). And the resolutions for strain and temperature are 24.28 $\mu\varepsilon$ and 0.49 °C, respectively. Eq. (5) shows that the sensing resolution can be improved by decrease the matrix determinant $|M|$. So the sensor performance may be optimized by choosing other kinds of TCFs.

We also experimentally investigated the performance of the proposed sensor by simultaneous measuring temperature and strain. Firstly, the applied strain was changed under a constant temperature of 42 °C. Then, the ambient temperature varied at a fixed strain of 533.32 $\mu\varepsilon$. The measured values of strain and temperature were plotted in Fig. 8. The maximum errors of strain and temperature were found to be 37.41 $\mu\varepsilon$ and 0.732 °C, respectively. Compared to the calculated resolutions of 24.28 $\mu\varepsilon$ and 0.49 °C, the performance were degraded due to the finite accuracy of the devices of the OSA, heating oven, digital thermometer, and translation stage.

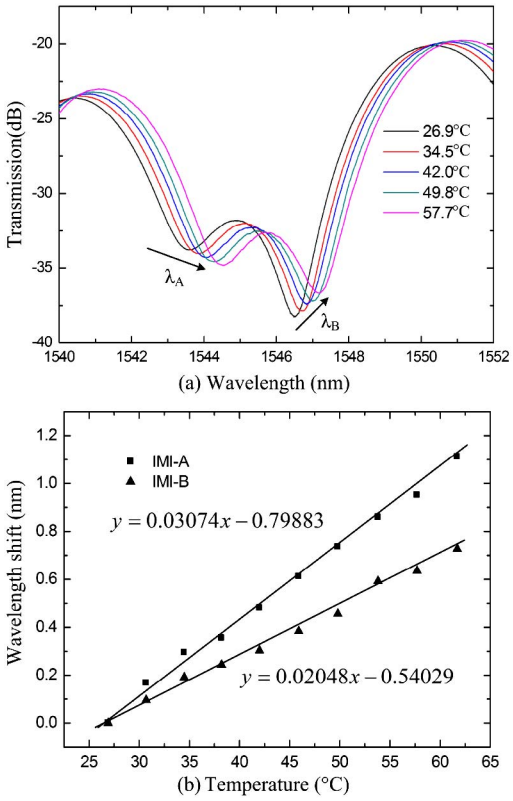

Fig. 7. (Color online) (a) Measured spectral response to temperature; (b) The wavelength shifts of the IMI-A and IMI-B as a function of temperature.

The strain sensitivity (−1.03 pm/$\mu\varepsilon$) of the proposed sensor is comparable with that of the FBG sensor (0.766 pm/$\mu\varepsilon$) [2], and the temperature sensitivity is measured to be 30.74 pm/°C, which is about three times higher than that of the FBG sensor (~10 pm/°C). Compared with the grating-based methods of discrimination between strain and temperature, the whole fabrication process of our proposed sensor is only fiber splicing and it can be achieved by a commercial fiber fusion splicer. So the sensor has the advantages of simple operation, low cost, and high sensitivity. Compared to the method of using high-birefringence fiber loop, the proposed sensor with the sensor length of several centimeters offers the merits of small in size, and it can be applied in miniature situation sensing. The sensor structure shows relatively high insertion loss, however, it does not affect the measurement accuracy, because we measure the resonant wavelength shift. Thus an optimized splicing program could be studied to reduce the insertion loss. Furthermore, the sensing sensitivities and resolution can be enhanced by using other kinds of fibers. In addition, the proposed sensor structure is much easier to fabricate than a grating-based sensor therefore it may finds potential applications in dual-parameter sensor.

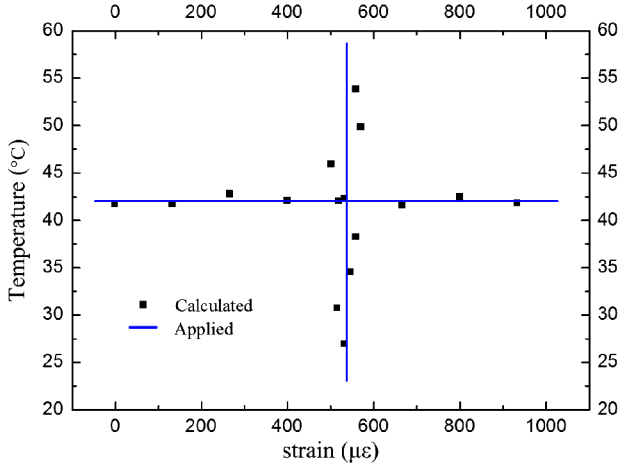

Fig. 8. (Color online) Sensor output obtained by Eq. (6) for the applied strain and temperature.

4. Conclusion

We have demonstrated a fiber-optic sensor configuration for discrimination of strain and temperature. The sensor head is formed by serially connecting two sections of TCFs. The resonant wavelengths of the TCF-based IMIs show different sensitivities to the variations of strain and temperature. From the sensitivity coefficient matrix, simultaneous measurement of strain and temperature can be determined. The sensing sensitivities of strain and temperature are −1.03 pm/$\mu\varepsilon$ and 30.74 pm/°C, and the measured strain and temperature resolutions are 37.41 $\mu\varepsilon$ and 0.732 °C, respectively. The fabrication of the proposed sensor is very simple and it also features the advantages of low cost and high sensitivity, which indicates that the proposed sensing structure exhibits great potential for dual-parameter measurement.

The work was jointly supported by the National Nature Science Fund of China (No. 60972032 and No. 60632010) and the National "863" Hi-tech Project of China.

References

1. E. Chehura, S. W. James, and R. P. Tatam, "Temperature and strain discrimination using a single tilted fibre Bragg grating," Opt. Commun. **275**, 344–347 (2007).
2. Y. Miao, B. Liu, and Q. Zhao, "Simultaneous measurement of strain and temperature using single tilted fibre Bragg grating," Electron. Lett. **44**, 1242–1243 (2008).
3. B. O. Guan, H. Y. Tam, H. L. W. Chan, C. L. Choy, and M. S. Demokan, "Discrimination between strain and temperature with a single fiber Bragg grating," Microw. Opt. Technol. Lett. **33**, 200–202 (2002).
4. O. Frazao and J. L. Santos, "Simultaneous measurement of strain and temperature using a Bragg grating structure written in germanosilicate fibres," J. Opt. Pure Appl. Opt. **6**, 553–556 (2004).
5. B. O. Guan, H. Y. Tam, X. M. Tao, and X. Y. Dong, "Simultaneous strain and temperature measurement using a superstructure fiber Bragg grating," IEEE Photon. Technol. Lett. **12**, 675–677 (2000).
6. H. J. Patrick, G. M. Williams, A. D. Kersey, J. R. Pedrazzani, and A. M. Vengsarkar, "Hybrid fiber Bragg grating/long period fiber grating sensor for strain/temperature discrimination," IEEE Photon. Technol. Lett. **8**, 1223–1225 (1996).

7. M. G. Xu, J. L. Archambault, L. Reekie, and J. P. Dakin, "Discrimination between strain and temperature effects using dual-wavelength fiber grating sensors," Electron. Lett. **30**, 1085–1087 (1994).
8. G. P. Brady, K. Kalli, D. J. Webb, D. A. Jackson, L. Reekie, and J. L. Archambault, "Simultaneous measurement of strain and temperature using the first and second-order diffraction wavelengths of Bragg gratings," IEE Proc. Optoelectron. **144**, 156–161 (1997).
9. S. Magne, S. Rougeault, M. Vilela, and P. Ferdinand, "State-of-strain evaluation with fiber Bragg grating rosettes: application to discrimination between strain and temperature effects in fiber sensors," Appl. Opt. **36**, 9437–9447 (1997).
10. G. Y. Sun, D. S. Moon, and Y. Chung, "Simultaneous temperature and strain measurement using two types of high-birefringence fibers in Sagnac loop mirror," IEEE Photon. Technol. Lett. **19**, 2027–2029 (2007).
11. O. Frazao, J. L. Santos, and J. M. Baptista, "Strain and temperature discrimination using concatenated high-birefringence fiber loop mirrors," IEEE Photon. Technol. Lett. **19**, 1260–1262 (2007).
12. D. P. Zhou, L. Wei, W. K. Liu, and J. W. Y. Lit, "Simultaneous measurement of strain and temperature based on a fiber Bragg grating combined with a high-birefringence fiber loop mirror," Opt. Commun. **281**, 4640–4643 (2008).
13. O. Frazão, L. M. Marques, S. Santos, J. M. Baptista, and J. L. Santos, "Simultaneous measurement for strain and temperature based on a long-period grating combined with a high-birefringence fiber loop mirror," IEEE Photon. Technol. Lett. **18**, 2407–2409 (2006).
14. Z. B. Tian, S. S. H. Yam, and H. P. Loock, "Single-mode fiber refractive index sensor based on core-offset attenuators, " IEEE Photon. Technol. Lett. **20**, 1387–1389 (2008).
15. L. V. Nguyen, D. Hwang, S. Moon, D. S. Moon, and Y. J. Chung, "High temperature fiber sensor with high sensitivity based on core diameter mismatch," Opt. Express **16**, 11369–11375 (2008).
16. Z. B. Tian, S. S. H. Yam, J. Barnes, W. Bock, P. Greig, J. M. Fraser, H. P. Loock, and R. D. Oleschuk, "Refractive index sensing with Mach-Zehnder interferometer based on concatenating two single-mode fiber tapers," IEEE Photon. Technol. Lett. **20**, 626–628 (2008).
17. R. Jha, J. Villatoro, G. Badenes, and V. Pruneri, "Refractometry based on a photonic crystal fiber interferometer," Opt. Lett. **34**, 617–619 (2009).
18. D. P. Zhou, L. Wei, W. K. Liu, Y. Liu, and J. W. Y. Lit, "Simultaneous measurement for strain and temperature using fiber Bragg gratings and multimode fibers," Appl. Opt. **47**, 1668–1672 (2008).
19. B. Dong, J. Z. Hao, C. Y. Liaw, B. Lin, and S. C. Tjin, "Simultaneous strain and temperature measurement using a compact photonic crystal fiber inter-modal interferometer and a fiber Bragg grating," Appl. Opt. **49**, 6232–6235 (2010).
20. D. Bo, D. P. Zhou, and L. Wei, "Temperature insensitive all-fiber compact polarization-maintaining photonic crystal fiber based interferometer and its applications in fiber sensors," J. Lightwave Technol. **20**, 1011–1015 (2010).
21. W. Jin, W. C. Michie, G. Thursby, M. Konstantaki, and B. Culshaw, "Simultaneous measurement of strain and temperature: Error analysis," Opt. Eng. **36**, 598–609 (1997).